

General relativistic polarized radiative transfer with inverse Compton scatterings

M. Mościbrodzka¹★

Department of Astrophysics/IMAPP, Radboud University, P.O. Box 9010, 6500 GL Nijmegen, The Netherlands

Accepted XXX. Received YYY; in original form ZZZ

ABSTRACT

We present `radpol` - a numerical scheme for integrating multifrequency polarized radiative transfer equations along rays propagating in a curved spacetime. The scheme includes radiative processes such as synchrotron emission, absorption, Faraday rotation and conversion, and, for the first time, relativistic Compton scatterings including effects of light polarization. The scheme is fully covariant and is applicable to model radio- γ -ray emission and its polarization from, e.g., relativistic jets and accretion flows onto black holes and other exotic objects described in alternative metric theories and modeled semi-analytically or with time-dependent magnetohydrodynamical simulations. We perform a few tests to validate the implemented numerical algorithms that handle light polarization in curved spacetime. We demonstrate application of the scheme to model broadband emission spectra from a relativistically hot, geometrically thick coronal-like inflow around a supermassive black hole where the disk model is realized in a general relativistic magnetohydrodynamical simulation.

Key words: black hole physics – MHD – polarization – radiative transfer – relativistic processes

1 INTRODUCTION

Complete models of emission spectra from magnetized plasmas falling onto a black hole event horizon, or onto a neutron star or ejected as jets where primary radiative processes are the synchrotron emission and the inverse-Compton process require incorporating information about light polarization. The polarized component of light carries additional to total intensity information about degree of ordering and strength of magnetic fields, geometry of the relativistic plasma, distribution function of particles in the plasma and gravitational fields. Including polarization in the radiative models enable us to investigate in more details the physical processes occurring in a variety of relativistic systems (Rees 1975).

Following pioneering works on strong gravitational effects on polarization vector (Balazs 1958; Connors & Stark 1977; Stark & Connors 1977; Connors et al. 1980; Ishihara et al. 1988) and polarized transport through various accretion flows with simplified geometries (Angel 1969; Laor et al. 1990; Haardt & Matt 1993; Matt et al. 1993; Poutanen & Vilhu 1993; Agol 1997; Agol & Krolik 2000; Dovčiak et al. 2004 and many others) recent focus is on developing numerical fully general relativistic models of polarized transfer through dynamical plasma models realized in general relativistic magnetohydrodynamical (GRMHD) simulations.

General relativistic *polarized* radiative transfer (RT) schemes are based on ray-tracing approach where RT equations are solved along geodesics lines that connect emission zone with an observer.

Most of the schemes include either synchrotron emission alone (Bromley et al. 2001; Broderick & Blandford 2003, 2004; Porth et al. 2011; Shcherbakov et al. 2012; Dexter 2016; Mościbrodzka & Gammie 2018; Pihajoki et al. 2018; Chan et al. 2019) or some other form of direct polarized emission (Chen et al. 2015).

An example of fully polarized general relativistic scheme Pandurata with direct synchrotron (or bremsstrahlung) emission and Compton scatterings off free relativistic electrons coupled to GRMHD simulations has been developed by Schnittman & Krolik (2013). More recently Zhang et al. (2019) developed a code MONK by adding polarization to `grmonty` - a general relativistic transfer scheme for synchrotron and Compton emission developed by Dolence et al. (2009) - but modeled polarized emission (due to scattering) in a toy model of a corona above a thin accretion disk in active galactic nuclei. Both of these codes use Walker-Penrose constant to parallel transport the polarization vector along the geodesics (Connors & Stark 1977) meaning that they are both limited to Kerr black holes described by Boyer-Lindquist coordinates. Both methods also completely neglect the effects of circular polarization, Faraday rotation and conversions effects and synchrotron emission and self-absorption within the relativistic plasma itself. All these radiative processes may be negligible for X-rays when these are produced by Compton scattered soft photons originating in a relativistically cold plasma, but these effects should be incorporated in models in case when a portion of X-ray emission in a relativistic system is produced by direct or scattered synchrotron emission, for example, from accelerated electrons or if one is interested in making con-

★ E-mail: m.moscibrodzka@astro.ru.nl

nections between emissions in high and low energies in relativistic systems.

For complete description of multiwavelength polarized emission models in this work we introduce a numerical scheme that takes into account: fully general relativistic RT of all Stokes parameters including synchrotron emission, synchrotron self-absorption, Faraday rotation, Faraday conversion and Compton scatterings of polarized light off free relativistic electrons. Our scheme is the first one build within completely covariant framework that will allow one to build radiative models in any metric and coordinate system in fully three dimensions. Thermal photons from cold plasma can be easily incorporated in the model, if necessary. Including scattering of photons off bound electrons would require small modifications of the scattering cross-sections and the polarization sensitive scattering kernel. Hence, the new scheme is suitable to model variety of relativistic configurations.

The structure of the article is as follows. In Sec 2, we recall equations for polarized RT in relativistic plasmas. In Sect.3, we describe the scheme developed to solve the polarized RT in three dimensions. In Sect. 4, we describe and carry out test of our polarization sensitive Compton scattering scheme and we compare the numerical results to known semi-analytic solutions. In Sect. 5 show comparison of the integrations of RT using the new scheme to results from existing schemes based on a complex plasma configuration - a hot accretion flow around Kerr black hole realized in three-dimensional GRMHD simulation. Sect. 6 gives a short summary.

2 EQUATIONS

2.1 Photons trajectories

Photon trajectories are described with null-geodesics equation

$$\frac{d^2 x^\mu}{d\lambda^2} = -\Gamma_{\alpha\beta}^\mu \frac{dx^\alpha}{d\lambda} \frac{dx^\beta}{d\lambda} \quad (1)$$

where $\frac{dx^\mu}{d\lambda} \equiv k^\mu$ is the electromagnetic wave four-vector, the affine parameter λ is defined through the geodesic equation, and Γ 's are the connection coefficients that account for curvature of a stationary metric. The metric itself is a parameter of a model.

2.2 Synchrotron processes

We consider polarized radiative transfer along geodesics through relativistic, fully ionized, magnetized plasma in which the dominating radiative transfer processes are synchrotron emission/absorption, Faraday effects and inverse-Compton process. The equations for evolution of Stokes parameters due to synchrotron emission/self-absorption and Faraday effects is:

$$\frac{d}{d\lambda} \begin{pmatrix} I \\ Q \\ U \\ V \end{pmatrix} = \begin{pmatrix} j_I \\ j_Q \\ j_U \\ j_V \end{pmatrix} - \begin{pmatrix} \alpha_I & \alpha_Q & \alpha_U & \alpha_V \\ \alpha_Q & \alpha_I & \rho_V & -\rho_U \\ \alpha_U & -\rho_V & \alpha_I & \rho_Q \\ \alpha_V & \rho_U & -\rho_Q & \alpha_I \end{pmatrix} \begin{pmatrix} I \\ Q \\ U \\ V \end{pmatrix} \quad (2)$$

where j_{IQUV} is the synchrotron emissivity, α_{IQUV} is the absorptivity and ρ_{QUV} is the Faraday rotation/conversion, and where the absence of subscript v implies that a term appears in invariant form, i.e. $j_I = j_{v,I}/v^2$, $\alpha_Q = v\alpha_{v,Q}$, and $\rho_V = v\rho_{v,V}$ and the derivative is understood to follow an individual photon in frequency space. Notice that Eq. 2 is written down in the rest-frame that is co-moving with the plasma, in which transfer coefficients are defined, and it does not describe how to parallel transport the polarization vector. The

covariant formulation of polarization vector transport is presented, e.g., in [Gammie & Leung \(2012\)](#) who re-wrote relativistic transport equation in terms of coherency tensor $N^{\alpha\beta}$:

$$k^\mu \nabla_\mu N^{\alpha\beta} = J^{\alpha\beta} + H^{\alpha\beta\gamma\delta} N_{\gamma\delta} \quad (3)$$

where ∇_μ is a covariant derivative, $J^{\alpha\beta}$ includes the emissivity coefficients, and $H^{\alpha\beta\gamma\delta}$ incorporates absorption and Faraday coefficients. The transformation of tensor components to Stokes parameters and vice-versa is trivial and requires defining an orthonormal tetrad $e_{(a)}^\mu$. The method of solving Eqs 2 and 3, its numerical implementation (ipole code) with extensive testings and comparison to independent scheme ([Dexter 2016](#)) and application to astrophysical problem is presented in our recent publication ([Mościbrodzka & Gammie 2018](#)).

2.3 Compton scattering

We consider Compton scatterings of synchrotron photons on free relativistic electrons (Synchrotron Self-Compton emission). The Compton scattering event is described in a tetrad in which electron is at rest, i.e., $e_{(0)}^\mu = p_e^\mu$ where p_e^μ is the four-momentum of an electron measured in the fluid co-moving frame. The z-axis is chosen to be aligned with the spatial part of the wavevector of the incident photon $e_3^\mu = k^\mu - \epsilon_e p_e^\mu$. The x and y axes (e_1^μ and e_2^μ) are chosen by orthogonalization.

The differential Klein-Nishina (KN) cross section for scattering of polarized photon on an unpolarized electron is ([Fano 1949](#), [Berestetskii et al. 1982](#)):

$$\frac{d\sigma^{KN}}{d\Omega} = \frac{1}{4} r_e^2 \left(\frac{\epsilon'_e}{\epsilon_e} \right)^2 \left[F_0 + F_{11} \xi_1 \xi'_1 + F_1 (\xi_1 + \xi'_1) + F_{22} \xi_2 \xi'_2 + F_{33} \xi_3 \xi'_3 \right] \quad (4)$$

where r_e is the electron classical radius, ϵ_e and ϵ'_e are incident and scattered energy of photon in units of $m_e c^2$, $\xi_{1,2,3}$ ($\xi'_{1,2,3}$) are normalized polarizations of incident (scattered) photon, i.e., $\xi_1 = Q/I$, $\xi_2 = U/I$, and $\xi_3 = V/I$, and F coefficients are elements of the Fano matrix ([Fano 1949, 1957](#))¹:

$$\begin{aligned} F_0 &= \frac{\epsilon'_e}{\epsilon_e} + \frac{\epsilon_e}{\epsilon'_e} - \sin^2 \theta' \\ F_1 &= \sin^2 \theta' \\ F_{11} &= 1 + \cos^2 \theta' \\ F_{22} &= 2 \cos \theta' \\ F_{33} &= \left(\frac{\epsilon'_e}{\epsilon_e} + \frac{\epsilon_e}{\epsilon'_e} \right) \cos \theta' \end{aligned} \quad (5)$$

where θ' is the polar angle of scattering and $d\Omega = \sin \theta' d\theta' d\phi'$. The dependency of the cross section on the azimuthal angle ϕ' is implicit since parameters ξ_{123} are defined in a coordinate system that is fixed to the scattering plane (plane normal to $\mathbf{k} \times \mathbf{k}'$). The transformation of fractional polarizations in a scattering event is

¹ Notice that [Berestetskii et al. 1982](#) (and many others) use different index numbers for fractional Stokes parameters and for the Fano matrix elements. Here we use indexing that is consistent with notation used in Sect. 2.2.

given by:

$$\begin{aligned}\xi'_1 &= \frac{F_1 + \xi_1 F_{11}}{F_0 + \xi_1 F_1} \\ \xi'_2 &= \frac{\xi_2 F_{22}}{F_0 + \xi_1 F_1} \\ \xi'_3 &= \frac{\xi_3 F_{33}}{F_0 + \xi_1 F_1}.\end{aligned}\quad (6)$$

and the transformation of the Stokes vector is described by:

$$\begin{pmatrix} I' \\ Q' \\ U' \\ V' \end{pmatrix} = \begin{pmatrix} \epsilon'_e \\ \epsilon_e \end{pmatrix}^2 \begin{pmatrix} F_0 & F_1 & 0 & 0 \\ F_1 & F_{11} & 0 & 0 \\ 0 & 0 & F_{22} & 0 \\ 0 & 0 & 0 & F_{33} \end{pmatrix} \begin{pmatrix} I \\ Q \\ U \\ V \end{pmatrix}\quad (7)$$

where the primed Stokes are Stokes parameters after scattering.

In Eq. 4 taking sum over all possible polarizations of the scattered photon ξ'_{123} one can obtain the total cross section as a function of incident photon polarization:

$$\frac{d\sigma^{KN}(\xi_{123})}{d\Omega} = \frac{1}{2} r_e^2 \left(\frac{\epsilon_e}{\epsilon'_e} + \frac{\epsilon'_e}{\epsilon_e} - (1 - \xi_1) \sin^2 \theta' \right).\quad (8)$$

Eq. 8 depends on linear polarization but is independent of Stokes U and V. For unpolarized incident photon and for elastic scattering ($\epsilon'_e = \epsilon_e$) Eq. 8 reduces to classical Thomson scattering cross section and Eq. 5 becomes Rayleigh scattering phase matrix.

Notice that the total KN cross section for incident polarized light (integrated over all scattering angles θ' and ϕ') is independent of polarization:

$$\begin{aligned}\sigma^{KN} &= \int \frac{d\sigma^{KN}}{d\Omega} d\Omega \\ &= \sigma^{TH} \frac{3}{4\epsilon_e^2} \left(2 + \frac{\epsilon_e^2(1 + \epsilon_e)}{(1 + 2\epsilon_e)^2} + \frac{\epsilon_e^2 - 2\epsilon_e - 2}{2\epsilon_e} \log(1 + 2\epsilon_e) \right).\end{aligned}\quad (9)$$

3 NUMERICAL METHOD

Our numerical methods to solve above equations extends existing unpolarized radiative transfer scheme `grmonty`, described in detail by Dolence et al. (2009). `grmonty` is a Monte Carlo general relativistic scheme simulating synchrotron emission and self-synchrotron and inverse-Compton scatterings. The code generates mock multiwavelength spectra for chosen plasma configuration and chosen metric tensor. Here we modify `grmonty` to also track light polarization along their original transport equations and to investigate how including polarization of light modifies the RT solutions. In what follows, we describe additions to the original scheme that allow us to follow polarization of synchrotron photons and polarization in relativistic Compton scatterings. Our new numerical scheme is referred as to `radpol`.

3.1 Polarized photons in Monte Carlo scheme: sampling and weights

The radiation field is represented by “superphotons”. Each superphoton is described by three quantities: coordinate x^μ , wave four-vector k^μ and weight w . The weight w is a scalar proportional to the number of photons in a single superphoton. To generate superphotons we follow exactly scheme described in Section 2 in Dolence et al. (2009). A modification is made to assign superphoton polarization state: namely each superphoton has now assigned four weights w_I, w_Q, w_U, w_V . Weight w_I (initially $w_I \equiv w$) is invariant

under Lorentz transformations and it is proportional to the invariant radiation specific intensity ($I_{\text{inv}} = I/\nu^3$ where ν is photon frequency). The three remaining weights are proportional to the “invariant” Stokes parameters:

$$w_Q \propto Q_{\text{inv}} \equiv Q/\nu^3, \quad w_U \propto U_{\text{inv}} \equiv U/\nu^3, \quad w_V \propto V_{\text{inv}} \equiv V/\nu^3.\quad (10)$$

While w_I is positive definite, w_Q, w_U, w_V can be negative so they do not have the same physical meaning as w_I , but they only quantify polarization of a superphoton.

Each superphoton k^μ and w_I are selected using rejection sampling based on plasma synchrotron emissivity for Stokes I, j_I . The remaining weights are defined using local synchrotron emissivities for Stokes Q, U and V, i.e., $w_Q = w_I j_Q / j_I$, $w_U = 0$, and $w_V = w_I j_V / j_I$. The initial superphoton wavevector k^μ and the polarization vector $\mathbf{w}_S = (w_I, w_Q, w_U, w_V)$ are defined in two different specific reference frames (tetrads).

The wavevector $k^{(a)}$ is sampled in an ortho-normal tetrad attached to the fluid element (plasma frame). The first tetrad basis vectors are $e_{(0)}^\mu = u^\mu$ and $e_{(3)}^\mu = b^\mu$, where b^μ is the magnetic field vector measured in the fluid frame. The other two basis vectors $e_{(1)}^\mu$ and $e_{(2)}^\mu$ are chosen via Gram-Schmidt orthonormalization procedure. The tetrad-to-coordinate basis Lorentz transformation for the superphoton wavevector is $k^\mu = e_{(a)}^\mu k^{(a)}$.

A different ortho-normal tetrad is built to tetrad-to-coordinate basis transformation for the polarization wavevector. This is because the synchrotron emissivities for Stokes parameters are defined in a special frame in which $j_U = 0$. This tetrad is defined as: $\tilde{e}_{(0)}^\mu = u^\mu$ and $\tilde{e}_{(3)}^\mu = k^\mu - \omega u^\mu$, where $\omega = -k^\mu u_\mu$ is the superphoton frequency measured by the observer with four-velocity u^μ . Notice, the third spatial basis element is a unit vector oriented parallel to the spatial component of the wavevector. Two other basis vectors are chosen via Gram-Schmidt orthonormalization procedure.

3.2 Parallel transport, absorption, Faraday rotation and conversion of a superphoton

N synchrotron superphotons is sampled and launched from the magnetized plasma. The plasma synchrotron emissivity is accounted for by assigning to each superphoton an initial polarization weights $\mathbf{w}_S = (w_I, w_Q, w_U, w_V)$. The weights are assigned in the plasma frame and translated into coherency tensor $N^{\alpha\beta}$ using the fluid tetrad. The parallel transport of polarization weights is then carried out by solving modified Eq. 3, i.e., leaving out all terms for plasma emissivity in transport equations:

$$k^\mu \nabla_\mu N^{\alpha\beta} = H^{\alpha\beta\gamma\delta} N_{\gamma\delta}\quad (11)$$

where coherency tensor $N^{\alpha\beta}$ now contains Stokes weights (instead of Stokes parameters.)² and the right-hand side of Eq. 11 accounts for self-absorption and Faraday effects only. The numerical method used to integrate Eq. 11 is adopted from `ipole` scheme (Mościbrodzka & Gammie 2018) who applied second-order split scheme for parallel transport plus source step to evolve $N^{\alpha\beta}$.

In the source step, we read-out \mathbf{w}_S from $N^{\alpha\beta}$ in the fluid frame and we solve (leaving out the emissivity coefficients accordingly):

$$\frac{d}{d\lambda} \begin{pmatrix} w_I \\ w_Q \\ w_U \\ w_V \end{pmatrix} = - \begin{pmatrix} \alpha_I & \alpha_Q & \alpha_U & \alpha_V \\ \alpha_Q & \alpha_I & \rho_V & -\rho_U \\ \alpha_U & -\rho_V & \alpha_I & \rho_Q \\ \alpha_V & \rho_U & -\rho_Q & \alpha_I \end{pmatrix} \begin{pmatrix} w_I \\ w_Q \\ w_U \\ w_V \end{pmatrix}\quad (12)$$

² $N^{\alpha\beta}$ relates to the Stokes weights \mathbf{w}_S is a same way as it relates to the standard Stokes parameters

Following [Mościbrodzka & Gammie \(2018\)](#) arguments we assume that transfer coefficients in Eq. 12 are constant along a single step on geodesics. In such case, Eq. 12 has simple solution:

$$\begin{pmatrix} w_I \\ w_Q \\ w_U \\ w_V \end{pmatrix}(\lambda) = O_{AB}(\lambda - \lambda_0) \begin{pmatrix} w_I \\ w_Q \\ w_U \\ w_V \end{pmatrix}(\lambda_0) \quad (13)$$

where analytic expression for operator $O_{AB}(\lambda - \lambda_0)$ has been found by [Landi Degl'Innocenti & Landi Degl'Innocenti \(1985\)](#). Also notice that operator O_{AB} is dimensionless so that \mathbf{w}_S can have arbitrary units. For unpolarized superphotons, i.e., $w_{QUV} = 0$, the Eq. 13 becomes:

$$\frac{dw_I}{d\tau_a} = -w_I, \quad (14)$$

where

$$d\tau_a = \alpha_l C d\lambda \quad (15)$$

and $C \equiv Lh/m_e c^2$ is a constant that depends on units of λ and k^μ . Quantity L is the lengthscale associated with a given physical problem, e.g., for RT around black hole, $L \equiv GM/c^2$. In the limit of unpolarized transport our new method is consistent with solutions originally implemented in `grmonty` because neither the parallel transport step nor the Lorentz transformations from coordinate frame to plasma frame (and vice versa) affect superphoton weight w_I (w_I is a scalar proportional to the number of photon quanta in a given superphoton).

3.3 Scattering of polarized radiation on relativistic electrons

When transporting light along geodesics an optical depth for Compton scattering, τ_{sc} , is computed. The optical depth for scattering is defined as

$$d\tau_{sc} = \alpha_{sc} C d\lambda \quad (16)$$

where α_{sc} is the Lorentz invariant scattering opacity given by integrating total KN cross section (Eq.9) over the assumed electron distribution function. In the event of scattering the wavevector k^μ and coherence tensor $N^{\alpha\beta}$ are Lorentz boosted into the plasma frame where for a given k_{plasma}^μ an electron energy and momentum is sampled from an isotropic electron distribution function. Given electron four-momentum in the plasma frame we construct another tetrad, defined within the plasma tetrad, in which the electron is at rest ($e_i^\mu = p_e^\mu$), the incident photon wavevector is aligned with spatial component of the third tetrad basis vector $e_3^\mu = k_{plasma}^\mu - \epsilon_e p_e^\mu$ where $\epsilon_e = -k_{plasma}^\mu p_{e,\mu}$ is the incident photon energy measured in the electron rest-frame. Basis vector e_2^μ and e_1^μ are chosen via orthonormalization. Two angles describe the scattered photon beam $\theta' \in (0, \pi)$ and $\phi' \in (0, 2\pi)$. Basis vector e_2^μ defines azimuthal scattering angle $\phi' = \pi/2$ and if the photon gets scattered along e_3^μ - then the polar scattering angle $\theta' = 0$.

We simulate Compton scattering in the electron frame as follows. 1) We sample the cosine of polar angle $\cos(\theta')$ and azimuthal ϕ' angle of scattered superphoton from uniform distributions. Azimuthal angle defines the scattering plane. 2) We rotate \mathbf{w}_S with respect to that azimuthal angle and calculate $\xi_1 = w_Q/w_I$. 3) The energy of scattered superphoton ϵ'_e is computed from kinematic relation: $\epsilon'_e = 1/(1 - \cos\theta + 1/\epsilon_e)$. In case of incident photon with small energy in comparison to electron rest mass energy ($\epsilon_e \ll 1$) the scattering becomes elastic independently of scattering angle. 4) Given ϵ_e , ϵ'_e , and scattering angles ϕ' and θ' , the transformation of a

polarization vector \mathbf{w}_S is done using Eq. 7 (notice that we do alter the w_I in a scattering event because the scattering angles are randomly chosen rather than drawn from the distribution function). 5) Given the new \mathbf{w}'_S we build a new coherency tensor of scattered photon that is transformed from electron to fluid and then from fluid to coordinate frame for further parallel transport with the scattered wavevector. 6) In the final step of the scattering simulation, a wavevector of scattered beam is constructed with:

$$\begin{aligned} k^{(0)} &= \epsilon'_e \\ k^{(1)} &= \epsilon'_e \sin\theta' \cos\phi' \\ k^{(2)} &= \epsilon'_e \sin\theta' \sin\phi' \\ k^{(3)} &= \epsilon'_e \cos\theta' \end{aligned} \quad (17)$$

which is transformed from electron rest-frame to fluid frame and then from fluid frame to coordinate frame where it is parallel transported along geodesic equation.

3.4 Polarized spectrum recorded by an external observer

To construct observed polarized spectrum of the plasma model, we build a polarimetric “detector”. The detector is another tetrad defined as: $e_{(0)}^\mu = u_d^\mu$ where u_d^μ is the detector four-velocity defined by user (by default we set a stationary observer). The detector is located at a distance r_d from the origin of the utilized coordinate system. The detector occupies solid angle $d\Omega \equiv d\phi_d d\theta_d \sin(\theta_d)$, where the angular size is given by $\Delta\phi_d$ and $\Delta\theta_d$ and detector it is centered at $(\theta_{d,0}, \phi_{d,0})$, which are free parameters.

Measuring polarization of a superphoton requires projection of the $N^{\alpha\beta}$ into the detector tetrad and extraction of weights for each Stokes parameter. Our polarimetric detector has energy bins from radio to γ -ray frequencies. All sampled superphotons are independent of one another, hence in case of multiple superphotons falling into the same energy bin, their Stokes parameters (or weights in this case) can be summed over ([Chandrasekhar 1960](#)). We translate \mathbf{w}_S measured in the detector frame into luminosities using following relations:

$$\begin{aligned} \nu L_{I,\nu,i} &= \frac{4\pi}{\Delta\Omega\Delta t} \frac{1}{\Delta \ln \nu} \sum_j w_{I,j} h\nu_j, \\ \nu L_{Q,\nu,i} &= \frac{4\pi}{\Delta\Omega\Delta t} \frac{1}{\Delta \ln \nu} \sum_j w_{Q,j} h\nu_j, \\ \nu L_{U,\nu,i} &= \frac{4\pi}{\Delta\Omega\Delta t} \frac{1}{\Delta \ln \nu} \sum_j w_{U,j} h\nu_j, \\ \nu L_{V,\nu,i} &= \frac{4\pi}{\Delta\Omega\Delta t} \frac{1}{\Delta \ln \nu} \sum_j w_{V,j} h\nu_j. \end{aligned} \quad (18)$$

4 SIMPLE TEST PROBLEMS

We carry out two simple tests to validate the polarization sensitive scattering kernel. Both tests assume Minkowski spacetime.

4.1 Scattering of unpolarized beam off one relativistic electron

In the first test we consider a monochromatic, unpolarized beam of light scattering off a single electron with a fixed $p_e^\mu = (1, 0, 0, 0)$. Here we consider scattering in Thomson regime. Fig. 1 shows maps

of Stokes I and Stokes Q of scattered light as a function of scattering angle θ' and ϕ' . The numerical calculations agree with theoretical prediction, scattered light on electron at rest is more linearly polarized when scattered at 90 degrees and the polarization angle depends on ϕ' angle. For very small and close to maximum scattering polar angles the scattered light remains unpolarized.

4.2 Scattering of polarized beam off a population of relativistic electrons

In the second test we consider a monochromatic, polarized beam of light scattering off a population of relativistic electrons described by Maxwell-Jüttner distribution function parameterized by dimensionless electron temperature $\Theta_e \equiv k_B T_e / m_e c^2$. The analytic solutions to this problem has been found by [Bonometto et al. \(1970\)](#). We describe these solutions and their limitations in detail in the appendix. In Fig. 2 we show agreement between the numerical solutions and the analytical expectations for thermal electrons with $\Theta_e = 100$ and various incident beam linear and circular polarizations. We show results for light scattered in direction $(\theta', \phi') = (85^\circ, 0)$.

5 COMPLEX TEST PROBLEMS

5.1 Astrophysical problem

Our numerical radiative transfer scheme inherits many of the numerical methods from `grmonty` and `ipole` codes, both of which have been extensively tested assuming simple and complex plasma conditions in flat, twisted and curved spacetimes (see e.g. [Mościbrodzka & Gammie 2018](#), [Mościbrodzka 2019](#)). The main application of the `radpol` scheme is modeling multiwavelength emission from relativistic jets and accretion flows around compact objects. Here we test the performance of `radpol` and compare it to its "parent" codes using a model of complex accretion flow. The background stationary spacetime is described by Kerr metric parameterized with dimensionless spin parameter $a_* \equiv Jc/GM^2$ with $|a_*| < 1$ (where M and J are, respectively, the mass and the angular momentum of a black hole) and Kerr-Schild coordinate system. The underlying magnetized plasma dynamics is simulated using 3D GRMHD code. We consider radiative transfer through a geometrically thick, relativistically hot disk accreting onto spinning ($a_* = 0.9375$) black hole ([Gammie et al. 2003](#)).

To construct mock observations of a simulation, one has to specify the free parameters of the RT model: the central black hole mass M_{BH} , accretion rate \dot{M} (which scales the dimensionless density and magnetic field strength), electron model (here we assume strong coupling between heavy ions and electrons and that electrons are described by the Maxwell-Jüttner distribution function) and the observer's viewing angle i measured with respect to the coordinate $\theta = 0$ direction. We assume $M_{\text{BH}} = 6.5 \times 10^9 M_\odot$, $\dot{M} = 4 \times 10^{-4} [M_\odot \text{yr}^{-1}]$ and $i = 60^\circ$ (see [Mościbrodzka et al. 2016, 2017](#) for details). These parameters are close to ones used to model emission from the core of M87 galaxy. However, here we do not attempt to model any particular observations, but only demonstrate the scheme performance.

5.2 Comparison to ipole: polarized synchrotron spectra

`ipole` is an imaging ray tracing code in which radiative transfer equations are solved along null-geodesics that terminate at a

"detector" at some large distance from the central object where a polarization map at a chosen observing frequency is constructed. In `ipole` simulations the synchrotron emission, synchrotron self-absorption and Faraday rotation and conversion are included but the inverse-Compton scatterings are not accounted for. Hence we can check consistency of `radpol` and `ipole` in the direct synchrotron emission only. `ipole` is producing images at a given frequency, to construct spectra we generate frames for many frequencies and integrate intensity of all Stokes parameters over each polarimetric map.

In Fig. 3, we show synchrotron spectrum in all Stokes I, Q, U and V produced by both codes. The figure shows that results from `radpol` converge to those from `ipole`. The agreement between the codes is at the level of 10 per cent in Stokes I, which is reasonable given the second order integration scheme implemented in both codes. Codes show less agreement in low frequency, self-absorbed portion of the synchrotron spectrum where the fractional polarizations are much lower (due to selfabsorption and Faraday rotation effects) than the errorbars on Stokes I. We expect that the differences decrease for smaller step size on the geodesics.

5.3 Comparison of SED to original grmonty scheme

Here we calculate broadband SED (synchrotron+Compton) emitted by a model of a accretion disk model described in Sect. 5.1. In Fig. 4, we show comparison of total intensities of synchrotron emission from the relativistic accretion flow using original unpolarized radiative transfer scheme `grmonty` and our new fully polarized radiative transfer scheme. The two spectra agree with each other within 10 per cent error and the best agreement, within 1 per cent, is in the optically thin part of the synchrotron spectrum. The differences decrease with the size of the step on geodesics. We conclude that our new numerical scheme `radpol` produces spectra that are consistent with those from `grmonty` scheme.

In Fig. 4 along with the total intensity emission we also show the expected total linearly and circularly polarized emission from the hot accretion flow. The circular polarization is low in the present model and therefore it is quite noisy. The total linear polarization of the SED is less than 10 per cent except at very high energy emission at $\nu > 10^{22}$ Hz where the signal-to-noise decreases.

6 SUMMARY

We developed a Monte Carlo general relativistic radiative transfer scheme `radpol`. The new scheme is capable of tracking polarization in the radiative transfer solutions, including synchrotron emission/absorption, Faraday effects and relativistic Compton scatterings. We have tested the new polarimetric scattering kernel against semi-analytic solutions and we compared the spectra emitted by a relativistic accretion disk model to spectra produced by other radiative transfer codes based on the same model. We find that the new code produces polarized synchrotron spectra that converge to those from `ipole` code. However the signal-to-noise of the Monte Carlo simulations should be improved to reach a better agreement in optically thick part of the synchrotron hump.

In this work, we consider scattering only on electrons with thermal relativistic (Maxwell-Jüttner) energy distribution function. Additional physics such as synchrotron emission and synchrotron self-Compton scatterings on non-thermal electron distributions described by a power-law or κ functions ([Livadiotis & McComas 2013](#)) can be now easily incorporated and tested.

The new scheme is fully covariant and it has several possible applications. It can be used to model spectra of relativistic systems such as gamma-ray bursts jets, X-ray binary systems or active galactic nuclei cores and jets for which polarization information is available at low and high energies. The scheme can be also used to estimate under what circumstances the Compton scattered radiation can be polarized. Such estimates can be now done for highly non-trivial plasma and magnetic field configurations.

Finally, since the total intensity and the geometry of the high energy radiation field depend on the polarization state of the seed photons certain high energy processes should be discussed in context of the current models. These processes, that are not included in the present work but ought to be discussed in a follow-up work, include: electron-positron pair productions (e.g. [Mościbrodzka et al. 2011](#)), double Compton process ([Gould 1984](#)), and stimulated Compton emission (e.g., [Reinisch 1976](#)).

ACKNOWLEDGEMENTS

I would like to thank Charles Gammie for his constructive and thoughtful comments on this work. I also would like to thank Ryuichi Kurosawa for discussions of Monte Carlo methods. This research has made use of NASA's Astrophysics Data System Bibliographic Services.

REFERENCES

- Agol E., 1997, PhD thesis, UNIVERSITY OF CALIFORNIA, SANTA BARBARA
- Agol E., Krolik J. H., 2000, [ApJ](#), **528**, 161
- Angel J. R. P., 1969, [ApJ](#), **158**, 219
- Balazs N. L., 1958, [ApJ](#), **128**, 398
- Berestetskii V., Lifshitz E.M. P. L., 1982, Quantum electrodynamics
- Bonometto S. A., Saggion A., 1973a, *Astrophys. Lett.*, **13**, 193
- Bonometto S. A., Saggion A., 1973b, *Astrophysical Letters*, **13**, 193
- Bonometto S., Cazzola P., Saggion A., 1970, *Astronomy and Astrophysics*, **7**, 292
- Broderick A., Blandford R., 2003, [MNRAS](#), **342**, 1280
- Broderick A., Blandford R., 2004, [MNRAS](#), **349**, 994
- Bromley B. C., Melia F., Liu S., 2001, [ApJ](#), **555**, L83
- Chan J. Y. H., Wu K., On A. Y. L., Barnes D. J., McEwen J. D., Kitching T. D., 2019, [MNRAS](#), **484**, 1427
- Chandrasekhar S., 1960, *Radiative transfer*
- Chen B., Kantowski R., Dai X., Baron E., Maddumage P., 2015, [ApJS](#), **218**, 4
- Connors P. A., Stark R. F., 1977, [Nature](#), **269**, 128
- Connors P. A., Piran T., Stark R. F., 1980, [ApJ](#), **235**, 224
- Dexter J., 2016, [MNRAS](#), **462**, 115
- Dolence J. C., Gammie C. F., Mościbrodzka M., Leung P. K., 2009, [ApJS](#), **184**, 387
- Dovčiak M., Karas V., Matt G., 2004, [MNRAS](#), **355**, 1005
- Fano U., 1949, *Journal of the Optical Society of America (1917-1983)*, **39**, 859
- Fano U., 1957, *Reviews of Modern Physics*, **29**, 74
- Gammie C. F., Leung P. K., 2012, [ApJ](#), **752**, 123
- Gammie C. F., McKinney J. C., Tóth G., 2003, [ApJ](#), **589**, 444
- Gould R. J., 1984, [ApJ](#), **285**, 275
- Haardt F., Matt G., 1993, [MNRAS](#), **261**, 346
- Ishihara H., Takahashi M., Tomimatsu A., 1988, [Phys. Rev. D](#), **38**, 472
- Krawczynski H., 2012, [ApJ](#), **744**, 30
- Landi Degl'Innocenti E., Landi Degl'Innocenti M., 1985, [Sol. Phys.](#), **97**, 239
- Laor A., Netzer H., Piran T., 1990, [MNRAS](#), **242**, 560
- Livadiotis G., McComas D. J., 2013, [Space Science Reviews](#), **175**, 183

- Matt G., Fabian A. C., Ross R. R., 1993, [MNRAS](#), **264**, 839
- Mościbrodzka M., 2019, [A&A](#), **623**, A152
- Mościbrodzka M., Gammie C. F., 2018, [MNRAS](#), **475**, 43
- Mościbrodzka M., Gammie C. F., Dolence J. C., Shiokawa H., 2011, [ApJ](#), **735**, 9
- Mościbrodzka M., Falcke H., Shiokawa H., 2016, [A&A](#), **586**, A38
- Mościbrodzka M., Dexter J., Davelaar J., Falcke H., 2017, [MNRAS](#), **468**, 2214
- Pihajoki P., Mannerkoski M., Nätilä J., Johansson P. H., 2018, [ApJ](#), **863**, 8
- Porth O., Fendt C., Meliani Z., Vaidya B., 2011, [ApJ](#), **737**, 42
- Poutanen J., Vilhu O., 1993, [A&A](#), **275**, 337
- Rees M. J., 1975, [MNRAS](#), **171**, 457
- Reinisch G., 1976, [Physica B+C](#), **81**, 339
- Schnittman J. D., Krolik J. H., 2013, [ApJ](#), **777**, 11
- Shcherbakov R. V., Penna R. F., McKinney J. C., 2012, [ApJ](#), **755**, 133
- Stark R. F., Connors P. A., 1977, [Nature](#), **266**, 429
- Zhang W., Dovčiak M., Bursa M., 2019, [ApJ](#), **875**, 148

APPENDIX A: SCATTERING OF A PHOTON BEAM ON AN ARBITRARY DISTRIBUTION OF ELECTRONS: SEMI-ANALYTIC SOLUTION

[Bonometto et al. \(1970\)](#) (see also [Bonometto & Saggion 1973a](#) and [Bonometto & Saggion 1973b](#)) found a semi-analytic expression for the intensity of a unidirectional and monochromatic photon beam polarized along ε scattered by an isotropic distribution of electrons into k' direction (\hat{k}') into polarization ε' :

$$J_{\varepsilon'} = K\gamma_{min} \frac{\varepsilon'}{\varepsilon} \left\{ \left[\varepsilon \cdot \varepsilon' + \frac{(\hat{k} \cdot \varepsilon')(\hat{k}' \cdot \varepsilon)}{1 - \cos \theta'} \right]^2 (\Sigma_1 + \Sigma_2) + \Sigma_2 \right\} \quad (\text{A1})$$

where $K = 1/2hc r_0^2 \text{ cm}^{-3}$, and $\gamma_{min} = \sqrt{\frac{1}{2} \frac{\varepsilon'}{\varepsilon} \frac{1}{1 - \cos \theta'}}$ is the minimum Lorentz factor required to produce scattered photons with energy ε' . The quantities \hat{k} , \hat{k}' are directions of incident and scattered photon beam and ε and ε' are their polarizations, measured in the plasma frame. Summing Eq. A1 over two orthogonal polarizations gives the total intensity of the Compton scattered radiation:

$$J_{\varepsilon'} + J_{\varepsilon'_\perp} = K\gamma_{min} \frac{\varepsilon'}{\varepsilon} (\Sigma_1 + 3\Sigma_2). \quad (\text{A2})$$

The quantities Σ_{12} are given in integral forms:

$$\Sigma_1 = \int_0^1 m(\gamma) \left(x^2 - \frac{1}{x^2} + 2 \right) dx \quad (\text{A3})$$

$$\Sigma_2 = \int_0^1 m(\gamma) \frac{(1-x^2)^2}{x^2} dx \quad (\text{A4})$$

where

$$x = \frac{\gamma_{min}}{\gamma} \quad (\text{A5})$$

and where $m(\gamma)$ depends on arbitrary chosen isotropic electron distribution function:

$$m(\gamma) = \frac{dn_e}{d\gamma} \gamma^{-2}. \quad (\text{A6})$$

[Bonometto et al. \(1970\)](#) show (see also [Krawczynski 2012](#)) that fractional polarization of the scattered beam is:

$$\xi'_1 = \delta \frac{\Sigma_1 + \Sigma_2}{\Sigma_1 + 3\Sigma_2}. \quad (\text{A7})$$

where δ is the fractional polarization of the incident beam with linear polarization parallel to the scattering plane (solutions for

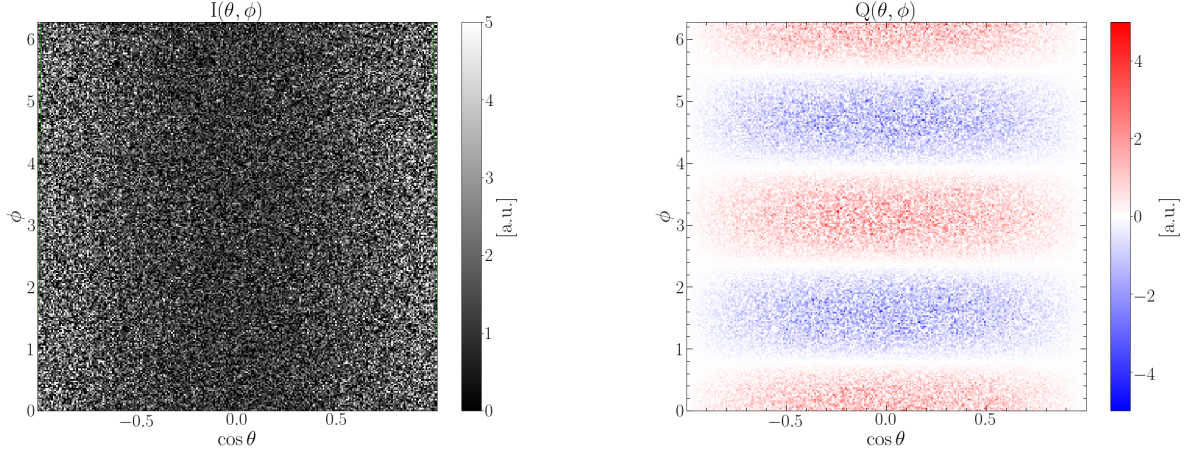


Figure 1. Stokes I and Q of Thomson scattered initially unpolarized light off electron at rest as a function of the scattering polar and azimuthal angle. The Stokes parameters have arbitrary units.

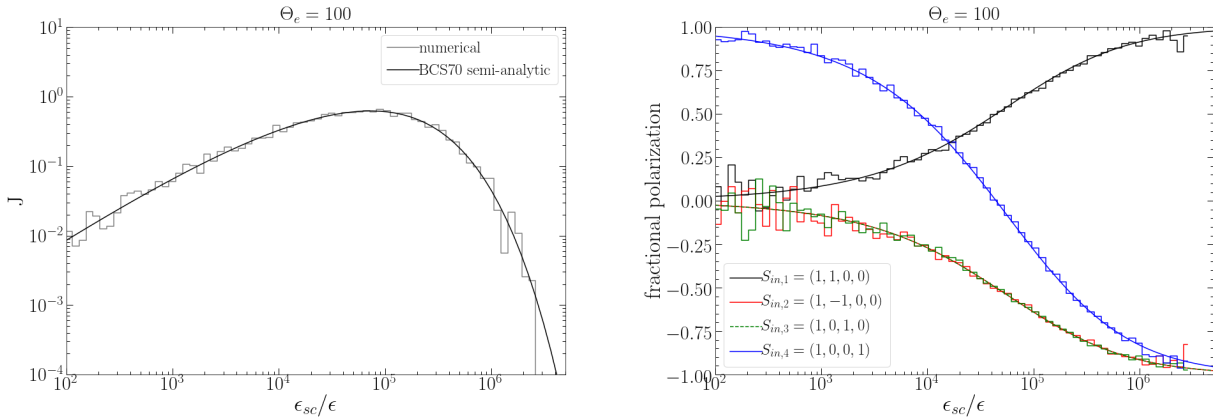


Figure 2. Analytical expectation from Bonometto et al. (1970) (lines) and numerical results (histograms) for intensity (left panel) and fractional polarizations (right panel) of unidirectional, monochromatic light scattered off thermal relativistic electrons parameterized with $\Theta_e = 100$ into angle $(\theta', \phi') = (85^\circ, 0)$. The initial beam energy in the ‘fluid’ frame is $\epsilon = 2.5 \times 10^{-11}$ to ensure that the scatterings in electron frame are elastic. We consider four cases when incident beam has different polarization state, S_{in} . The scattered light fractional polarizations agree with theoretical predictions of Bonometto et al. (1970). In this problem, the scattered light total intensity does not depend on the initial beam polarization and agrees with theoretical predictions.

other incident polarization directions or circular polarization are also available, see Bonometto et al. 1970). Notice that these semi-analytic solutions are derived only for Thomson scatterings but are applicable to any electron distribution function.

Let’s consider scattering on Maxwell-Jüttner distribution of electrons:

$$m(\gamma) = \frac{\gamma \sqrt{\gamma^2 - 1}}{K_2(1/\Theta_e)\Theta_e} e^{-\gamma/\Theta_e} \gamma^{-2}. \quad (\text{A8})$$

The integrals $\Sigma_{1,2}$ are evaluated using Gaussian Quadratures in *Gnu Scientific Libraries*. A photon beam with direction along z-axis ($\hat{k} = (0, 0, 1)$) has initial energy $\epsilon = 2.5 \times 10^{-11}$. In Fig. 2 (left panel) we plot the expected semi-analytic (Eq. A2) and numerical (produced by our Monte Carlo code) SEDs for electron temperatures $\Theta_e = 100$ for photons scattered in direction described by set of angles $(\theta', \phi') = (85^\circ, 0)$. In this test, we considered four cases

with different polarizations of incident beam: $S_{in,1} = (1, 1, 0, 0)$, $S_{in,2} = (1, -1, 0, 0)$, $S_{in,3} = (1, 0, 1, 0)$, and $S_{in,4} = (1, 0, 0, 1)$ where S_i is the Stokes parameter. $S_{1,2,3}$ describes a beam that is initially parallel, perpendicular, 45 angle linear polarization and S_4 is circularly polarized. In Fig. 2 (right panel) shows scattered photon polarization in four cases; the numerical results are consistent with theoretical expectations.

This paper has been typeset from a $\text{\TeX}/\text{\LaTeX}$ file prepared by the author.

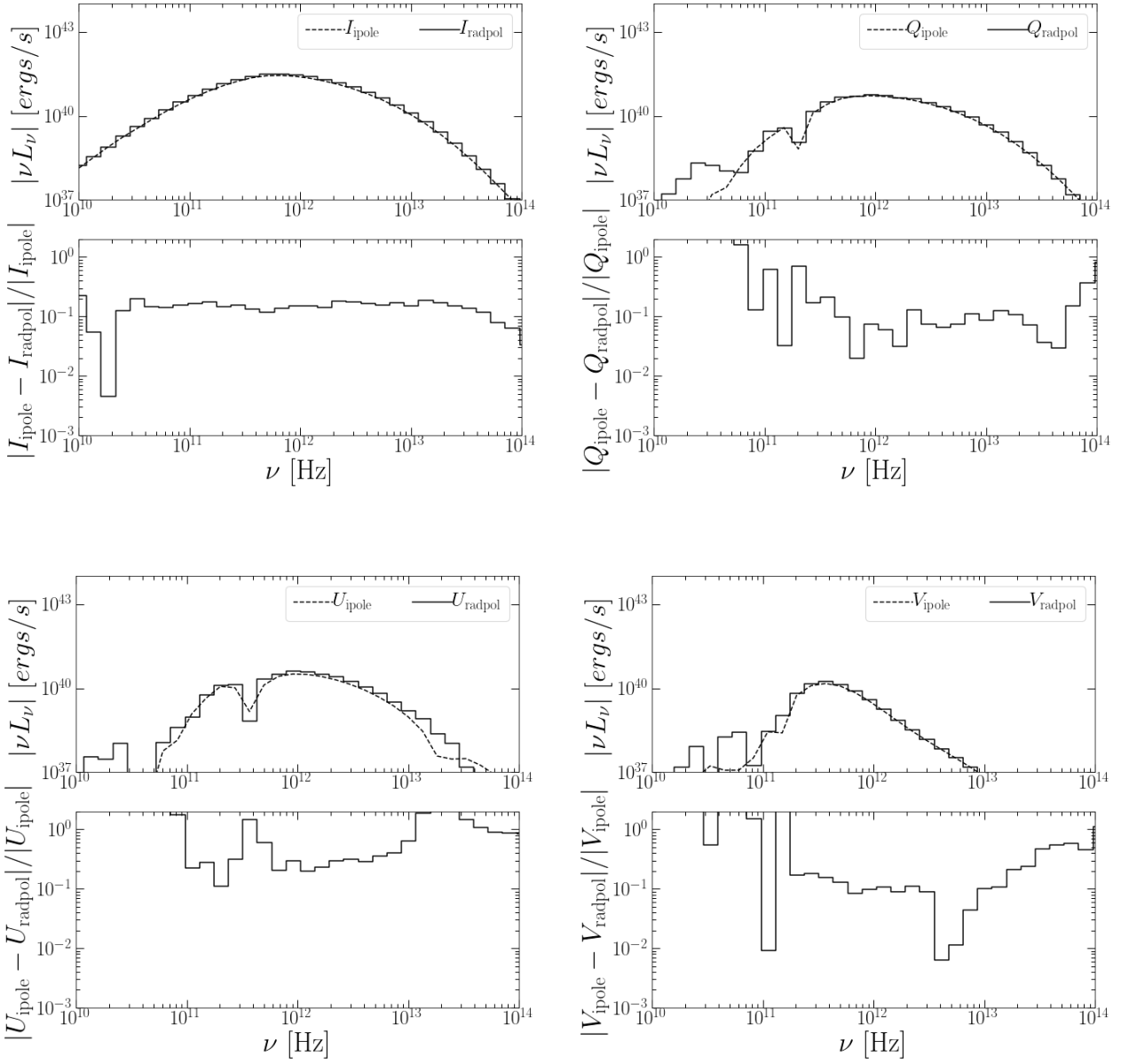


Figure 3. Comparison of the synchrotron spectrum computed with `ipole` ($IQUV_{\text{ipole}}$) and `radpol` ($IQUV_{\text{radpol}}$). Codes agree well in Stokes I, the differences is at the level of ~ 10 per cent. If the fractional linear or circular polarization becomes less than 10 per cent the difference in Stokes QUV becomes large.

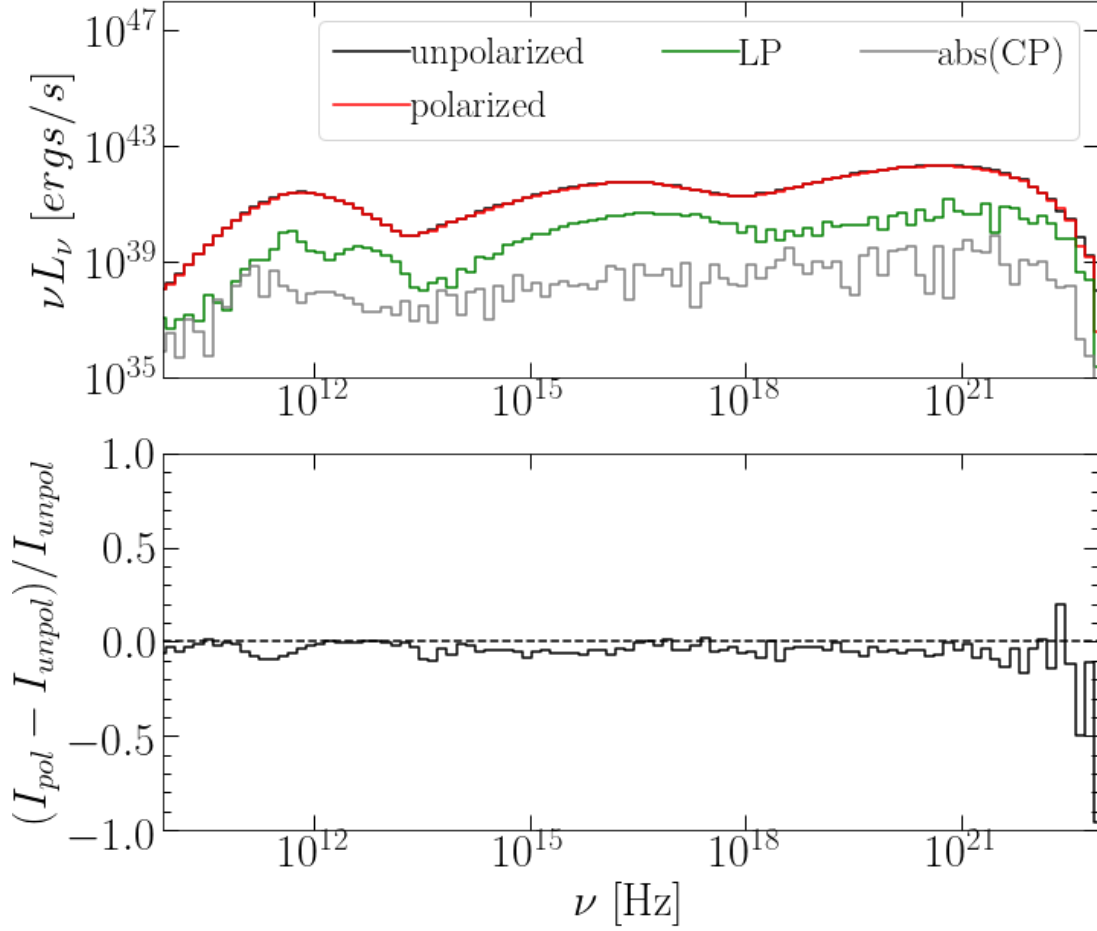


Figure 4. Comparison of the total intensity synchrotron and Compton spectrum emitted by a hot accretion flow around a supermassive black hole. Unpolarized spectra are computed using scalar transport in `grmonty` code and the new fully polarized spectra are from the presented `radpol` scheme. For the chosen parameter of the integration (step size on geodesics) the relative difference between the two distinct schemes is less than 10 per cent for most of the wavelengths. The largest difference is measured at very high energies, near the exponential cut-off of the SED. Here we also present the linearly and circularly polarized flux of the model.